



**UNIVERSITY
OF TURKU**

This is a self-archived – parallel-published version of an original article.

This article has been accepted for publication in Monthly notices of the royal astronomical society ©: 2023 .Published by Oxford University Press on behalf of the Royal Astronomical Society. All rights reserved.

AUTHOR	Phillipps S, Bellstedt S, Bremer MN, De Propris R, James PA, Casura S, Liske J, Holwerda BW
TITLE	Galaxy And Mass Assembly (GAMA): the dependence of star formation on surface brightness in low-redshift galaxies
YEAR	2022
DOI	http://dx.doi.org/10.1093%2Fmnras%2Fstac3440
VERSION	Publisher's PDF
CITATION	Phillipps, S et al. "Galaxy And Mass Assembly (GAMA): The Dependence of Star Formation on Surface Brightness in Low Redshift Galaxies." <i>Monthly notices of the Royal Astronomical Society</i> (2022): n. pag. Web.

Galaxy And Mass Assembly (GAMA): the dependence of star formation on surface brightness in low-redshift galaxies

S. Phillipps¹,^{*} S. Bellstedt^{1,2}, M. N. Bremer,¹ R. De Propris^{1,3,4}, P. A. James,⁵ S. Casura⁶, J. Liske⁶ and B. W. Holwerda^{1,7}

¹*Astrophysics Group, School of Physics, University of Bristol, Tyndall Avenue, Bristol BS8 1TL, UK*

²*ICRAR, University of Western Australia, 35 Stirling Highway, Crawley, WA6009, Australia*

³*Finnish Centre for Astronomy with ESO, University of Turku, Finland, Vesilinnantie 5, FI-21400, Turku, Finland*

⁴*Department of Physics and Astronomy, Botswana International University of Science and Technology, Private Bag 16, Palapye, Botswana*

⁵*Astrophysics Research Institute, Liverpool John Moores University, IC2, Liverpool Science Park, 146 Brownlow Hill, Liverpool L3 5RF, UK*

⁶*Hamburger Sternwarte, Universität Hamburg, Gojenbergsweg 112, D-21029 Hamburg, Germany*

⁷*Department of Physics and Astronomy, University of Louisville, 102 Natural Science Building, Louisville KY 40292, USA*

Accepted 2022 November 18. Received 2022 November 3; in original form 2022 August 26

ABSTRACT

The star-formation rate in galaxies is well known to correlate with stellar mass (the ‘star-forming main sequence’). Here, we extend this further to explore any additional dependence on galaxy surface brightness, a proxy for stellar mass surface density. We use a large sample of low-redshift ($z \leq 0.08$) galaxies from the Galaxy And Mass Assembly survey which have both spectral energy distribution (SED) derived star-formation rates and photometric bulge-disc decompositions, the latter providing measures of disc surface brightness and disc masses. Using two samples, one of galaxies fitted by a single component with Sérsic index below 2 and one of the discs from two-component fits, we find that once the overall mass dependence of star-formation rate is accounted for, there is no evidence in either sample for a further dependence on stellar surface density.

Key words: galaxies: photometry – galaxies: star formation – galaxies: structure.

1 INTRODUCTION

Star formation and its history are key elements in the evolution of any galaxy. Elucidating the factors which determine the star-formation rate (SFR) in a given galaxy at any particular time is therefore key to our understanding of global galaxy evolution.

It is well established that the SFR depends on the stellar mass (M_*) of a galaxy; galaxies which have significant ongoing star formation follow a ‘star-forming main sequence’ (Noeske et al. 2007; Speagle et al. 2014, and many others) in a plot of SFR against M_* . As the relationship is not linear, there is a corresponding correlation between specific star-formation rate (sSFR; the SFR per unit mass) and mass (e.g. Davies et al. 2016, 2019, and references therein).

A number of authors (e.g. Ellison et al. 2008; Mannucci et al. 2010; Lara-Lopez et al. 2013; Salim et al. 2014; Telford et al. 2016) have extended this to explore a possible three-way correlation between galaxy (gas phase) metallicity, mass, and SFR (at both low and high redshift), with some finding that at given mass the metallicity is higher in lower SFR galaxies, while others argue that the variation in metallicity is entirely a function of mass (e.g. Sanchez et al. 2013, 2015). Most recently, Thorne et al. (2022) do not see a strong dependence of the mass–metallicity relation on SFR. On the other hand, Peng, Maiolino & Cochrane (2015) showed a dependence of stellar metallicity on SFR, which they took as evidence for the strangulation model of star formation reduction. Recent works by Curti et al. (2020) and Bellstedt et al. (2021) summarize the status

of fits to a mass–metallicity–SFR plane, the latter finding that the residual effect of SFR on metallicity (or vice versa) is lessened at small look-back times (low z) in galaxies such as those studied here.

Given that SFR depends on the mass of stars already formed, another factor which has been suggested to play a role in the star-formation history (SFH) is the surface brightness (SB), or more physically the stellar surface density, of the star forming disc (e.g. Bell & de Jong 2000). Generically, this might be expected if the gravitational instability which leads to the star formation depends on the disc dynamical time or angular velocity (e.g. as summarized in Li, Mac Low & Klessen 2006), which for a given mass are obviously related to the radius and hence surface density. Similarly, self-regulating star-formation theories suggest that at fixed gas density, sSFR should depend on stellar or total mass surface density (Dopita 1985; Matteucci et al. 1989; Kennicutt & Evans 2012), while stability of gas discs in general depends on both the gaseous and stellar components (e.g. Jog & Solomon 1984; Elmegreen 1995; Dalcanton, Yoachim & Bernstein 2004; Martig et al. 2009).

However, much of the work and interest in this possible dependence has centred specifically on the class of low-surface brightness galaxies (LSBGs; e.g. Bell et al. 2000; Boissier et al. 2008), often with rather small samples of objects. Less attention has been paid to the effects of variations in SB amongst the full population of spiral discs (i.e. not just LSBGs), and the use of the large galaxy samples which have become available in recent years.

In the current paper, we use data from the Galaxy And Mass Assembly (GAMA) survey (Driver et al. 2011, 2022) to explore the connections between SFR and disc SB in spiral galaxies. Since we wish to concentrate on discs (assumed to provide the dominant

* E-mail: S.Phillipps@bristol.ac.uk

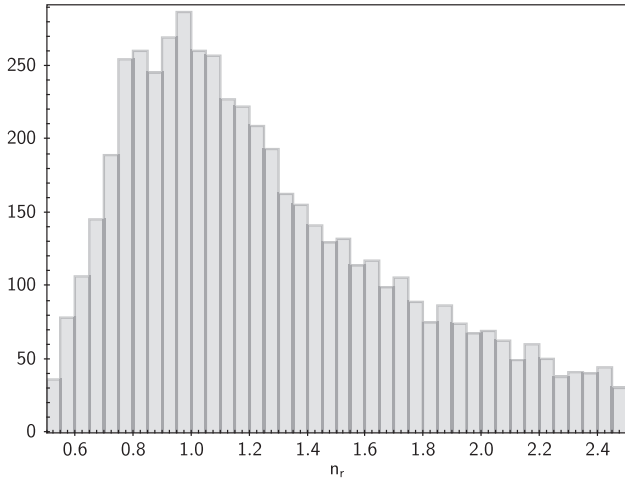


Figure 1. Distribution of r -band Sérsic indices n_r (excluding those above $n_r = 2.5$) for the single component fits.

contribution to the present-day star formation), we utilize the most recent photometric bulge-disc decompositions of GAMA galaxies presented by Casura et al. (2022). Our goal is to examine the correlations between the SFR and stellar surface density, if any exist, in the large statistically complete GAMA sample which enjoys both multiwavelength SFR estimates and uniformly determined profile fits.

Section 2 describes the GAMA spectroscopic and associated photometric data and the analysis of the radial SB profiles. Section 3 presents our main results on the variation of SFR with SB (and by proxy stellar surface density) and Section 4 discusses the results.

Where required we use a *Planck* 2015 cosmology (Planck Collaboration XIII 2016) with $H_0 = 67.8 \text{ km s}^{-1} \text{ Mpc}^{-1}$, $\Omega_m = 0.308$, $\Omega_\Lambda = 0.692$, as in Bellstedt et al. (2020b) from where we obtain our stellar masses and SFRs.

2 DATA AND SAMPLE

Our data arise from the spectroscopic GAMA survey and its allied multiwavelength photometric data sets. GAMA was a large, highly complete spectroscopic survey carried out with the AAOmega spectrograph on the *Anglo-Australian Telescope* which obtained redshifts for around 300 000 galaxies in three equatorial fields (G09, G12, and G15) and two southern fields (G02 and G23). Data releases are described in Driver et al. (2011), Liske et al. (2015), Baldry et al. (2018), and Driver et al. (2022).

The original optical photometry (and therefore selection) for GAMA was obtained from SDSS (specifically their DR8; Aihara et al. 2011); however, in the latest releases (Driver et al. 2022) this has been replaced by data from the Kilo-Degree Survey (KiDS; de Jong et al. 2013). KiDS is a wide-field imaging survey of the Southern sky in the optical broad-band filters u , g , r , and i carried out using the *VLT Survey Telescope (VST)* at the European Southern Observatory Paranal Observatory. The VISTA Kilo-degree Infrared Galaxy survey provides the corresponding near-infrared data in the Z , Y , J , H , and K_s bands (Edge et al. 2013; Wright et al. 2019). The GAMA II equatorial survey regions have been covered as of KiDS DR3.0 (de Jong et al. 2017). Using this photometry (see Bellstedt et al. 2020a), Driver et al. (2022) demonstrate that the GAMA spectroscopic sample in the equatorial regions is 95 percent complete to a KiDS r -band magnitude limit of $r = 19.65$.

In order to specifically concentrate on star-forming galaxy discs we require bulge/disc decomposition of two-component systems

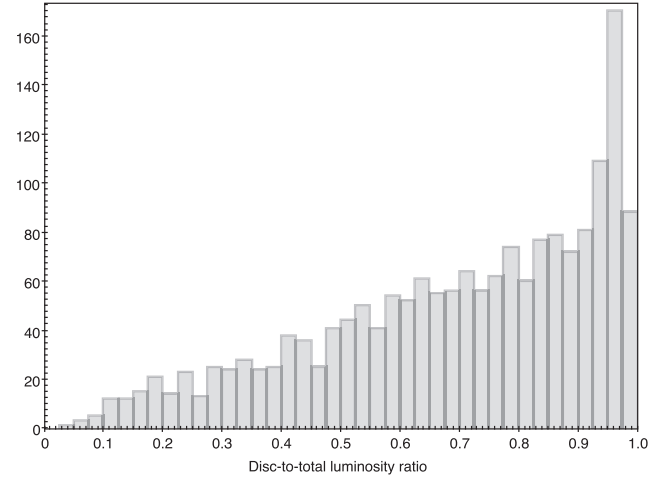


Figure 2. Distribution of r -band disc-to-total luminosity fractions for the galaxies fitted by two components.

where appropriate, i.e. for the earlier-type spirals. This limits us to relatively nearby (i.e. sufficiently well resolved) galaxies and we take the overall sample from Casura et al. (2022) which contains 13 096 galaxies out to $z = 0.08$.

Casura et al. (2022) fit both single Sérsic and two-component (point source or bulge plus exponential disc) SB profiles to the KiDS images by using the Bayesian two-dimensional fitting programme ProFit (Robotham et al. 2017). In what follows we utilize their choice of ‘recommended’ profile type, viz. their parameter JOINT-NCOMP; 1 (single component, with fitted Sérsic index n), 1.5 (unresolved point source + exponential), or 2 (bulge with fitted n + exponential). See Casura et al. (2022, section 3.3.2) for the discussion of this choice. A total of 8725 galaxies are well fit by one of these three options.

Of the galaxies best fit by a single Sérsic component, we choose those with $0.5 \leq n \leq 2.0$ as our ‘pure disc’ galaxy subsample. We will refer to these 4572 objects as Sample 1. The distribution of their r -band Sérsic indices is shown in Fig. 1. Changing the limit for discs to $n = 2.5$ has no significant effect on our subsequent results. Where morphological classifications exist for these galaxies (at $z < 0.06$; Moffett et al. 2016), as expected, these objects are nearly all classed as late-type spirals, with a subset of ‘little blue spheroids’ (i.e. star-forming dwarfs; see Moffett et al. 2019) at the low-mass end. Errors given in the Casura et al. catalogue are typically < 2 per cent in the half-light radius R_e and 0.02 magnitudes in r .

For the two-component fits (types 1.5 and 2), we simply use the disc component parameters with no further restrictions (these necessarily have $n = 1$). Fig. 2 shows the disc-to-total luminosity ratios in the r band for these 1790 galaxies, henceforth Sample 2. The remainder of the light is ascribed to a generic central ‘bulge’, whether resolved or not; 1405 are disc dominated with disc fraction above 0.5. Again quoted errors are typically < 0.02 magnitudes in r and 2 per cent in R_e .

3 CORRELATIONS BETWEEN SB AND STAR FORMATION

3.1 Surface brightness

For simplicity (and generality), we define our characteristic SB parameter μ to be the mean SB (in magnitudes per square arcsec) inside the effective (half-light) radius, i.e.

$$\mu \equiv \bar{\mu}_e = (m + 0.75) + 2.5 \log(\pi R_e^2) = m + 5 \log R_e + 2.0,$$

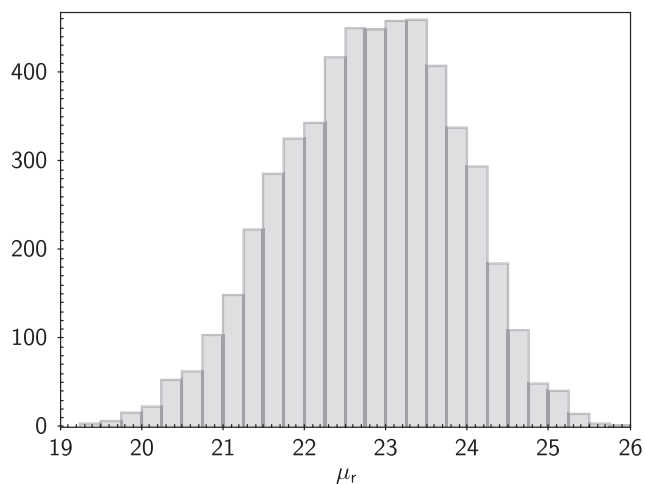


Figure 3. Distribution of r -band characteristic SB (in magnitudes per square arcsec) for the galaxies fitted by a single component and selected as discs.

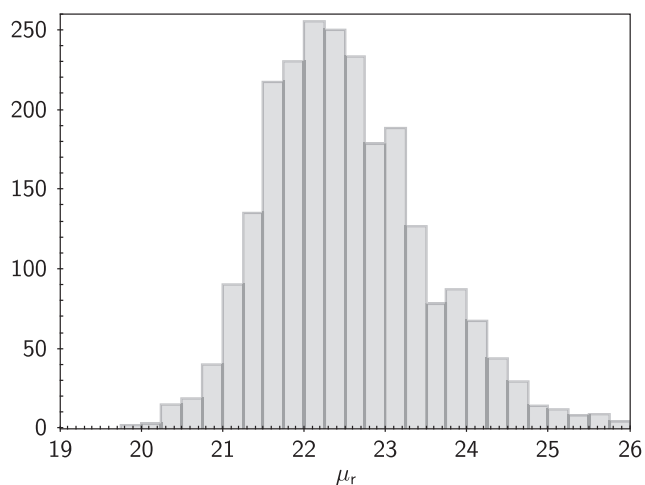


Figure 4. Distribution of r -band characteristic SB (in magnitudes per square arcsec) of the disc component for the galaxies fitted by two components.

where m is the total apparent magnitude in a given band and R_e is the corresponding effective radius, as given by the fitting procedure. Note that for Sample 1, these refer to the whole galaxy while for Sample 2 they are for the disc component.

Figs 3 and 4 show the overall distributions of μ (in the r band in this case) for the two samples. Given the quoted errors on the magnitude and effective radius, errors in μ_r are typically less than 0.05 magnitudes per square arcsec.

The simple prescription avoids the details of the galaxy and allows a comparison across galaxies with different values of the Sérsic index. Nevertheless, we can see that for a perfect $n = 1$ face-on exponential disc, for instance, μ is trivially related to the SB at R_e , μ_e , and to the central SB, μ_0 , through

$$\mu = \bar{\mu}_e = \mu_e - 0.70 = \mu_0 + 1.12$$

(Graham & Driver 2005).

Since we have used πR_e^2 in our definition, rather than the area of an elliptical image, πab ($= \pi R_e^2(b/a)$, where b/a is the axis ratio), we also automatically correct for the increase in apparent surface density with inclination of the disc (barring any small change in apparent r_e with inclination). We have not here made any correction for dust

extinction in the galaxy or its variation with inclination; we consider these later. We do, though, make the small $(1+z)^4$ correction for cosmological dimming.

While statistics of SB measurements are typically reported at blue wavelengths (Freeman 1970; Phillipps et al. 1987; O’Neil & Bothun 2020), here we concentrate on the r -band SB. This more accurately portrays surface mass density and avoids, or at least reduces, correlations forced purely by recently formed bright blue stars contributing a significant amount of the light. We also have i -band profiles, where the mass-to-light ratio is even less dependent on the SFR, and we use these as a consistency check, although the errors on the profile fit parameters are slightly larger than for the r band. We initially use our single Sérsic sample (with $n \leq 2$) and then repeat the analysis with the discs from the two-component fits.

3.2 Star-formation rates

There are numerous options for determining the SFR of the GAMA galaxies (Davies et al. 2016). Here, we make use of the SFRs derived by Bellstedt et al. (2020b) using the ProSpect software (Robotham et al. 2020) to fit a star-formation history model to the multiwavelength broad-band photometry. The data used to form the SED span the far-ultraviolet and near-ultraviolet from *GALEX*, *ugri* from the *VST*, *ZYJHKs* from *VISTA*, *W1–W4* from *WISE*, and *P100–S500* from *Herschel*.¹ The code then obtains a fit to the SED using a parametrized SFH and a physically motivated metallicity evolution. ProSpect also provides the present-day stellar mass of the galaxy. [Using the MAGPHYS (Da Cunha, Charlot & Elbaz 2008) derived SFRs from Driver et al. (2016) and Wright et al. (2016) does not materially affect our results]. From the ProSpect fits, errors are typically 15 per cent, i.e. 0.06 dex, in SFR (except at very low values) and 12 per cent (0.05 dex) in stellar mass.

We first consider the total SFR. Since it is well known that SFR depends strongly on stellar mass, we account for this before looking at the SB. Specifically we determine the slope m of a linear fit to $\log(\text{SFR})$ versus $\log(M_*)$, via an unweighted least-squares fit and use this to obtain a new parameter

$$\log(m\text{SFR}) = \log(\text{SFR}) - m\log(M_*),$$

which accounts for the overall mass dependence. For our single Sérsic sample, Sample 1, $m_1 = 0.85$, i.e. $m_1\text{SFR} = \text{SFR}/M_*^{0.85}$. For reference, Fig. 5 shows the ‘main sequence of star formation’ for Sample 1 in these terms; by design it shows no mass dependence. Note that the parameter $m_1\text{SFR}$ has the units of $M_\odot^{0.15} \text{yr}^{-1}$. It is not the same as using the sSFR, since the slope is slightly sublinear, i.e. sSFR decreases with mass. This result – for single-component disc-like galaxies only – is counter to the assertion of Abramson et al. (2014) that the slope of the usual main sequence of star formation deviates from unity only because of lower disc fractions at higher overall mass.

Notice that there are some quiescent galaxies, well below the main sequence, at all masses (though more so at high mass). These quiescent galaxies often appear as outliers in subsequent plots; however, removing them does not alter any of our conclusions. (Physically, the outliers tend to be preferentially towards higher masses, higher SBs, and larger bulge-to-disc ratios compared to the overall sample). As noted by Eales et al. (2017) and Oemler et al. (2017) (though see Salim et al. 2014; Holwerda et al. 2022), there is

¹GAMA Data Management Unit GAMAkidsVikingFIRv01; Driver et al. (2016). Note that not all galaxies have data beyond W2.

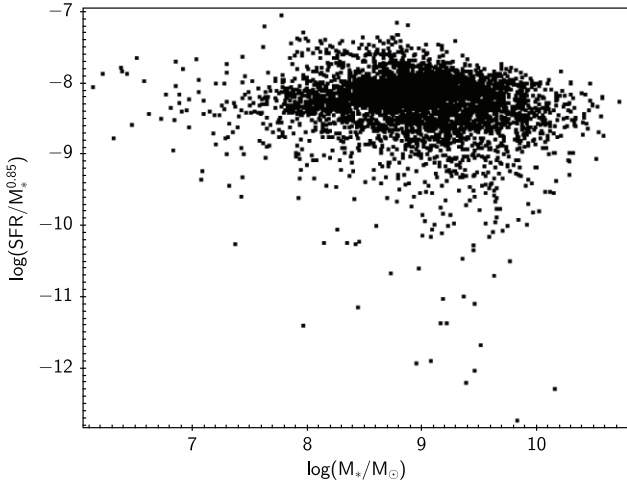


Figure 5. Variation of the mass-corrected SFR parameter, m_1SFR (in units of $M_{\odot}^{0.85} \text{ yr}^{-1}$), with stellar mass (in solar masses) for Sample 1.

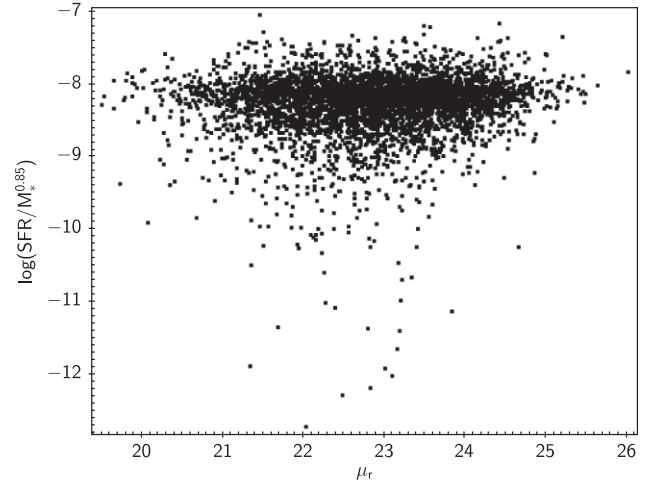


Figure 7. As Fig. 6 but for the mass-corrected SFR parameter m_1SFR (in units of $M_{\odot}^{0.85} \text{ yr}^{-1}$).

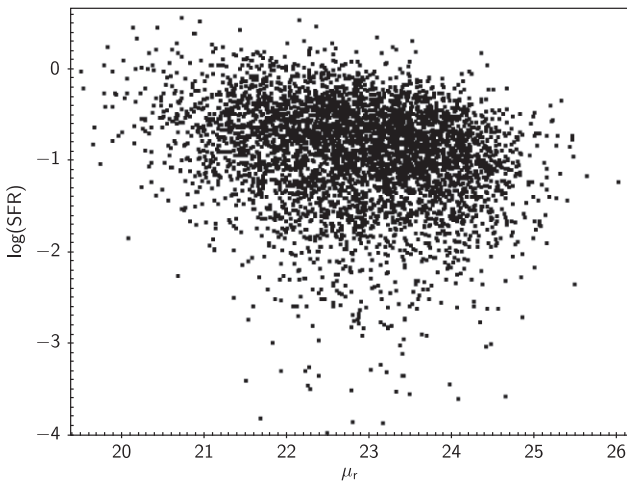


Figure 6. Variation of SFR (in $M_{\odot} \text{ yr}^{-1}$) with μ_r (in magnitudes per square arcsec) for Sample 1.

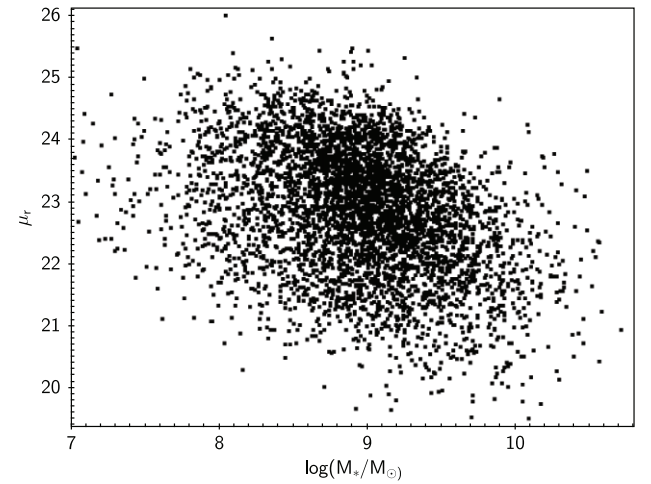


Figure 8. Variation of SB (in magnitudes per square arcsec) with stellar mass (in solar masses) for Sample 1.

no obvious ‘valley’ between main-sequence galaxies and quiescent galaxies when plotting SFR, as opposed to the case when using optical or ultraviolet (UV)-optical colour (e.g. Bremer et al. 2018, for GAMA). Errors in m_1SFR are typically <0.1 dex except at the very low levels.

We can now search for any remaining dependence on SB. Fig. 6 shows the overall dependence of SFR on μ_r ; however, Fig. 7 shows the equivalent plot for the mass-corrected m_1SFR . It is evident that while the SFR does vary with SB (e.g. Phillipps & Disney 1985; Bell & de Jong 2000; Hunter & Elmegreen 2004; O’Neil, Oey & Bothun 2007), once the primary mass dependence of the SFR is removed, there is no significant remaining dependence of SFR on SB (Pearson correlation coefficient $r = 0.09$), at least for galaxies in our sampled luminosity range. Note that Bell et al. (2012) found essentially the same result for low-redshift galaxies if we assume that $U - V$ colour (their fig. 7) is a proxy for the mass-normalized SFR.

One might, of course, argue that since SB is correlated with M_* , the primary dependence of SFR could be the one on mass density, as in Fig. 6, rather than mass. However, as is evident from Fig. 5, the correlation between SFR and mass is much tighter. The relation between SB and mass is actually also a rather broad one (see Fig. 8).

We can further confirm the lack of a relationship between SFR and SB by plotting SFR versus SB at a specific mass, say around the sample’s mass distribution peak at $10^9 M_{\odot}$, as shown in Fig. 9; again no correlation is seen (Pearson $r = 0.01$). As a further check, we find that splitting the sample into ‘round’ (fairly face-on) and ‘flat’ (more edge-on), above and below an axis ratio $b/a = 0.5$, or using the i -band SB, makes no difference to the (lack of) correlation ($r < 0.1$ in all cases).

In these plots, it is evident that there is a very wide range of SFR at a given SB, with neither the significantly star forming galaxies nor the quiescent galaxies showing a SB dependence. The errors in μ_r (~ 0.05 magnitudes per square arcsec) are very much smaller than would be required to blur out a real correlation.

Next, we repeat the analysis for the discs from the two-component fits, Sample 2. (Recall that there are fewer objects in this sample). We first determine the mass dependence of the SFR in the same way as before. To obtain the disc mass we have simply scaled the overall mass by the disc fraction in r -band luminosity (see Fig. 2), without attempting to allow for any differences in mass-to-light ratio, M/L , between the components. The mass-corrected SFR, m_2SFR , is defined similarly to the previous m_1SFR , though with a shallower

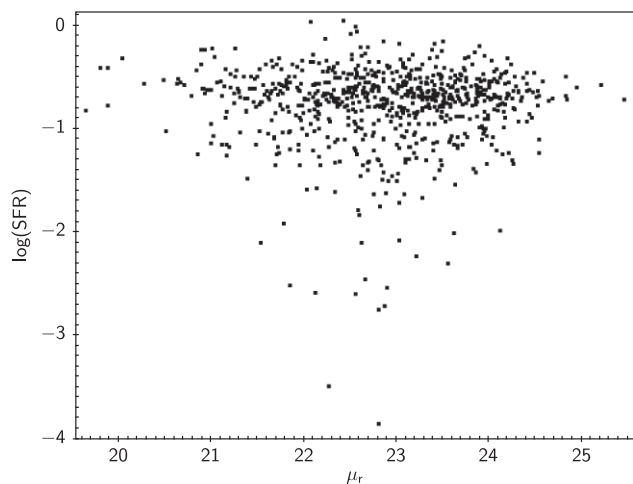


Figure 9. Variation of SFR (in $M_{\odot} \text{yr}^{-1}$) with μ_r (in magnitudes per square arcsec) for the single-component galaxies with mass between 10^9 and $10^{9.2} M_{\odot}$.

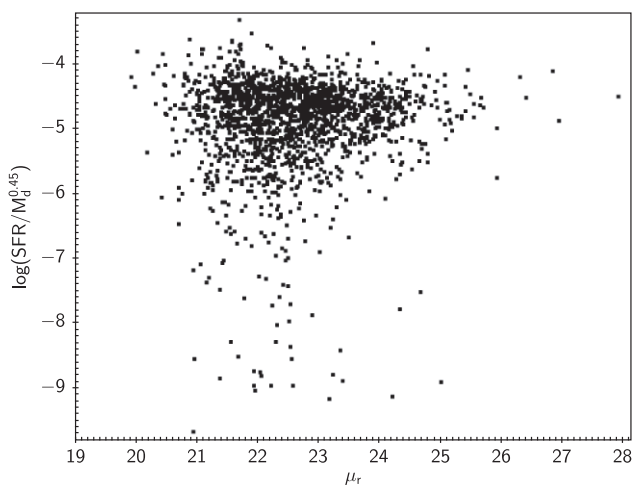


Figure 10. Variation of mass-corrected SFR parameter m_2SFR (in units of $M_{\odot}^{0.55} \text{yr}^{-1}$) with disc SB (in magnitudes per square arcsec) for Sample 2.

mass dependence, $m_2 = 0.45$, as empirically found for the ‘main sequence’ in this sample. (m_2SFR therefore has units of $M_{\odot}^{0.55} \text{yr}^{-1}$. Errors in m_2SFR are typically 0.08 dex).

Fig. 10 shows the distribution of m_2SFR against μ_r for these disc components. It is evident that again there is no systematic trend of m_2SFR with SB ($r = 0.05$), though the scatter increases towards the high-SB end, creating a rather wedge-shaped distribution. In particular, as noted above, the quiescent galaxies largely have high-SB discs. As for Sample 1, they are also primarily of high mass. (For completeness, Fig. 11 shows the overall distribution of SB with disc mass for Sample 2). Again, ‘round’ and ‘flat’ discs show the same lack of correlation. Similarly, the same distribution is seen for galaxies with resolved or with point-like ‘bulges’.

3.3 SFR surface density

It is, of course, well established that the surface density of SFR in galaxies, Σ_{sfr} , depends on their *gas* surface densities, Σ_{gas} (Schmidt 1959; Kennicutt 1998), though with a substantial scatter. In fact, a similar relationship, $\Sigma_{\text{sfr}} \propto \Sigma_{\text{gas}}^N$ with $N \simeq 1.4$, occurs within

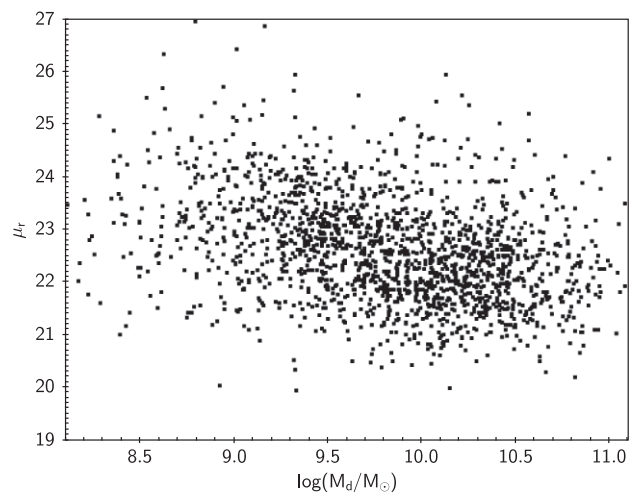


Figure 11. Variation of disc SB (in magnitudes per square arcsec) with disc mass (in solar masses) for Sample 2.

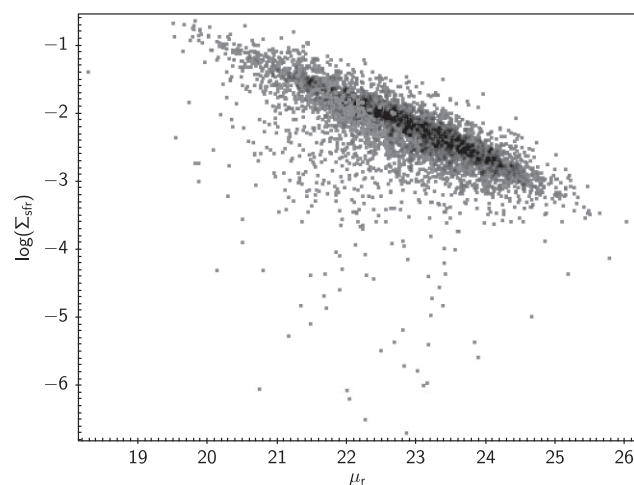


Figure 12. Variation of surface density of star formation, Σ_{sfr} (in units of $M_{\odot} \text{yr}^{-1} \text{kpc}^{-2}$) with SB (in magnitudes per square arcsec) for Sample 1.

individual galaxies (as seen in the radial profiles; e.g. Kennicutt 1989; Bigiel et al. 2008; Leroy et al. 2008), as well as between them. Barrera-Ballesteros et al. (2021) have recently summarized evidence that *within* individual galaxies Σ_{sfr} correlates with both Σ_{gas} (specifically the molecular mass) and the stellar surface density Σ_{*} .

One might therefore consider global correlations between galaxies of their SFR surface density with their characteristic *r*-band SB (again as proxy for the corresponding stellar mass surface density). Figs 12 and 13 show the variation of Σ_{sfr} with μ_r for the one-component fits and the discs of the two-component fits, respectively. In each case, the characteristic Σ_{sfr} , in units of $M_{\odot} \text{yr}^{-1} \text{kpc}^{-2}$, is calculated simply from the total SFR and the area corresponding to the effective radius. Errors in Σ_{sfr} are typically 0.07 dex.

This time we see very clear correlations between the SFR and SB. However, given the existence of a nearly linear correlation between SFR and luminosity (via the mass) for ‘main-sequence’ galaxies, dividing both SFR and L by (the same) area to obtain Σ_{sfr} and SB essentially guarantees a relation such as seen in Fig. 12. The less tight relation in Fig. 13 follows because the SFR– L relation is not linear for Sample 2 discs, so dividing each by area does not simply move points parallel to the relation. Even so, the correlations seen

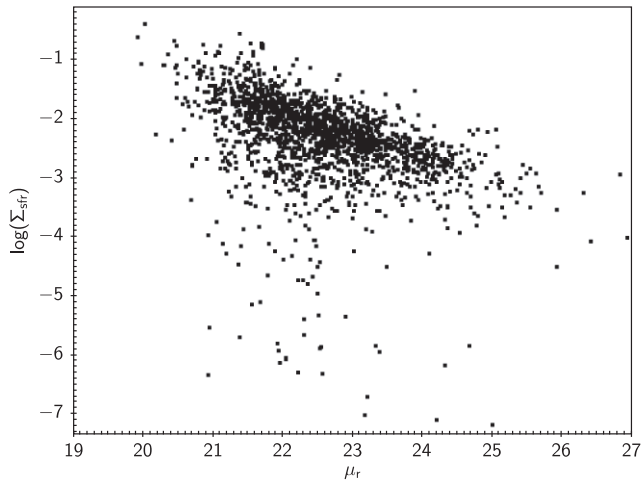


Figure 13. Variation of surface density of star formation Σ_{sfr} (in units of $M_{\odot} \text{ yr}^{-1} \text{ kpc}^{-2}$) with disc SB (in magnitudes per square arcsec) for Sample 2.

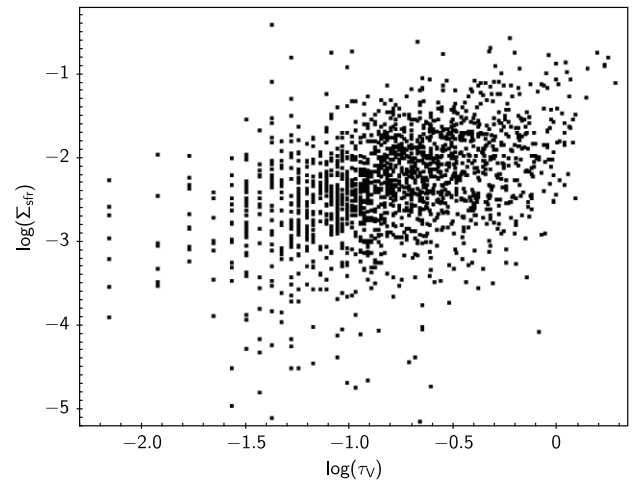


Figure 15. Variation of surface density of star formation, Σ_{sfr} , in units of $M_{\odot} \text{ yr}^{-1} \text{ kpc}^{-2}$, as a function of dust optical depth in the V band, τ_v , for discs of Sample 2.

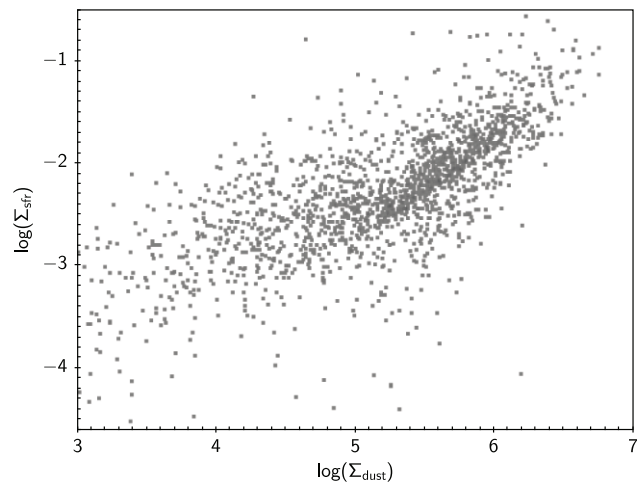


Figure 14. Variation of surface density of star formation Σ_{sfr} (in units of $M_{\odot} \text{ yr}^{-1} \text{ kpc}^{-2}$) as a function of dust mass surface density Σ_{dust} (in $M_{\odot} \text{ kpc}^{-2}$), for discs of Sample 2.

are clearly largely forced by the SFR– M_* relations and the use of the same areas when calculating Σ_{sfr} and μ_r .

3.4 Gas and dust

As an aside, although we do not have gas densities in the GAMA data, it is of interest to look at the dust content as a proxy (Eales et al. 2012), and indeed in its own right since correlations between SFR and dust mass are well established (da Cunha et al. 2008, 2010). In addition, Dalcanton et al. (2004) and Holwerda et al. (2019) suggest that the existence of dust lanes is related to disc gravitational instability. Fig. 14 shows (for Sample 2) Σ_{sfr} , as above in units of $M_{\odot} \text{ yr}^{-1} \text{ kpc}^{-2}$, versus the dust surface density Σ_{dust} in $M_{\odot} \text{ kpc}^{-2}$, the latter calculated in the same way from the total dust mass M_{dust} (as provided by ProSpect with typical errors of 20 per cent, 0.08 dex) and the effective radius. We can see that we retrieve a strong, near-linear correlation [as did Grootes et al. (2013), who also used $M_{\text{dust}}/R_{\text{c}}^2$ as a measure of Σ_{dust} and M_*/R_{c}^2 for Σ_* , from a detailed analysis of a small sample of GAMA galaxies]. However, this is again expected because of the

near-linear SFR– M_{dust} relation in da Cunha et al. (2010) (see also Rowlands et al. 2014; Beeston et al. 2018), for the same reason as for the $\Sigma_{\text{sfr}}-\mu_r$ relation in the previous section.

In this case, though, we can check whether there is a real correlation underlying Fig. 14 since we can alternatively plot the V-band disc optical depth τ_v derived from the MAGPHYS SED fitting (with typical errors of 20 per cent). This also represents the (diffuse) dust disc surface density but does not involve division by the area. Fig. 15 confirms that Σ_{sfr} does indeed vary with the dust surface density in this representation (and by presumption the gas surface density), as we would expect.² Though with a range of 2 dex at given τ_v , the plot is broadly compatible with a relation, $\Sigma_{\text{sfr}} \propto \tau_v$ for the significantly star-forming (‘main-sequence’) galaxies.

We should not, of course, expect there to be a perfect correspondence between the measured dust and the star-forming gas, not least because of the generally differently distributed atomic and molecular components; however, if we assume that the relationship between SFR and gas available for fuel is the fundamental one, then this correlation with Σ_{dust} implies that random variations in gas-to-dust ratio are small enough to keep the correlation intact, even though this ratio is known to itself vary with mass and a galaxy’s SFH (De Vis et al. 2017b), which will affect the slope we measure.

Fig. 16 then shows the dust optical depth τ_v against the SB μ_r . This shows that characteristic SB does not track the variation of (mean) surface density of dust (and gas) between galaxies (Pearson $r = 0.09$), consistent with its lack of correlation with SFR. De Vis et al. (2017a) show a similar lack of a significant relationship between Σ_* and UV extinction, if their separate group of very gas-rich, low-luminosity LSBGs is excluded.

4 DISCUSSION

What, then, should we make of the perhaps surprising main result aforementioned, that for galaxies of any given total stellar mass, the SFR (and also the surface density of star formation) does not depend on the r -band SB, and by inference the stellar mass surface density? There are a number of ways of looking at this.

²The vertical ‘stripes’ at low $\log(\tau_v)$ are due to the discrete values of τ_v in the MAGPHYS inputs.

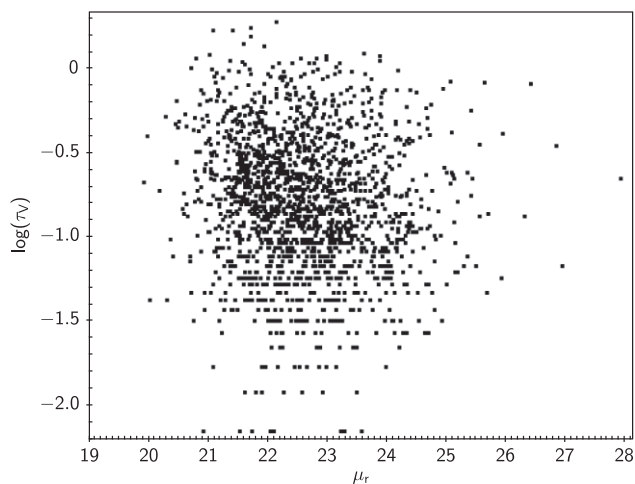


Figure 16. Variation of dust optical depth in the V band, τ_V , as a function of SB (in magnitudes per square arcsec) for discs of Sample 2.

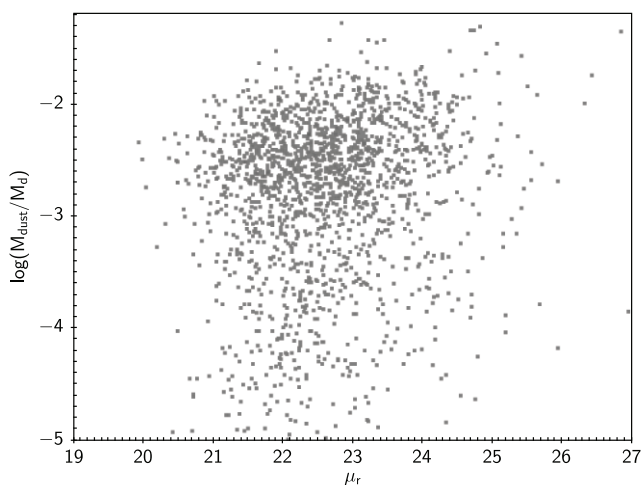


Figure 17. Variation of the ratio of dust mass to stellar disc mass with disc SB (in magnitudes per square arcsec) for Sample 2.

For instance, it is clear that if we take a set of (proto)disc galaxies with different initial surface densities of gas and let each evolve to similar remaining gas fractions (say a typical value for present-day spirals, around 10–20 per cent), then those with high stellar mass density will also have high (remaining) gas surface density and by implication high SFR, clearly counter to what is seen.

However, the non-linear slope of the Schmidt/Kennicutt relation between gas density and SFR implies that high-gas density systems convert a larger fraction of their gas into stars per unit time. Thus, we can imagine that the initially high-density systems have more quickly reduced their gas content and therefore fuel supply, so that, after a certain evolutionary time, their SFR is no higher than that of their initially lower density counterparts.

There would seem to be two testable implications of this. The high-initial density systems should, in this picture, clearly have high current stellar surface densities, and hence SB, and should also show (i) large average stellar population ages because of the high initial SFR (cf. MacArthur et al. 2004), and (ii) low gas fractions because of the rapid gas depletion (cf. Bell et al. 2003). Although, as above, the latter is not directly observable within our GAMA data, we might expect a corresponding low dust mass fraction.

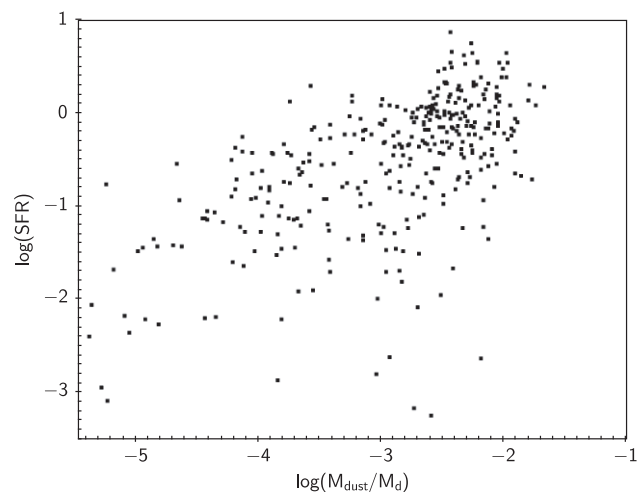


Figure 18. Variation of SFR (in $M_{\odot} \text{ yr}^{-1}$) with the ratio of dust mass to stellar disc mass for Sample 2 galaxies with disc SB limited to 22–22.5 magnitudes per square arcsec.

Prediction (i) has already been shown to hold for GAMA galaxies; Robotham, Bellstedt & Driver (2022) find that at given total mass, large galaxies (i.e. those with low mass surface density) do have younger stellar ages than smaller (higher surface density) galaxies. For prediction (ii), Fig. 17 shows the distribution of dust mass as a fraction of stellar disc mass against SB. (Errors in M_{dust}/M_d are around 0.13 dex). The galaxies with low dust mass fractions – and by implication low gas fractions – do tend to have high rather than low SB, but any overall trend is very weak ($r = 0.15$), high SB galaxies having a very wide range of dust-to-stellar mass ratios. Note that, although the outlier quiescent galaxies at low SFR are more likely to have low dust fraction, relative to the overall sample, removing them does not alter the appearance of Fig. 17 (i.e. it does not remove a significant number of the low-dust fraction galaxies), nor does it significantly alter the correlation coefficient.

Thus, we find only partial support for a toy model where the lack of dependence of the current SFR on stellar surface density is due to more rapid evolution of the high-density systems cancelling out the expected variation with original gas surface density.

An alternative way to look at this is to consider specifically the late evolution of galaxies of a given original (gas) surface density. Once the gas content has reduced to 10 per cent, for instance, any remaining star formation can only change the stellar surface density by a small factor (corresponding to ~ 0.1 magnitudes in SB). However, as the gas is used up and the gas content reduces to, say, 1 per cent, then by the Kennicutt relations we would expect the SFR to reduce by a factor ~ 30 . Thus, if we observe such galaxies at a variety of evolutionary stages (hence gas fractions) we should expect a wide range of SFR at a particular SB, as seen in our data, and that this variation should correlate with gas fraction.

To test this, galaxies have been selected from the two-component fit galaxies within the disc SB range $\mu_r = 22$ to 22.5 (the peak of the sample’s SB distribution in Fig. 4). Fig. 18 shows the relation between the ratio of dust-to-stellar mass, as proxy for gas fraction as above, and SFR. We see the expected correlation, for this simple model, that at fixed SB (and thus fixed *original* gas density), SFR increases with gas fraction. If we select out other SB ranges, the points entirely overlap with those for $\mu_r \simeq 22$.

We must therefore conclude that at fixed mass, the pre-existing stellar surface density (and therefore the original total surface density

of gas, barring any mergers) does not in any way modulate the current SFR.

ACKNOWLEDGEMENTS

GAMA is a joint European-Australasian project based around a spectroscopic campaign using the *Anglo-Australian Telescope*. The GAMA input catalogue is based on data taken from the Sloan Digital Sky Survey and the *UKIRT* Infrared Deep Sky Survey. Complementary imaging of the GAMA regions is being obtained by a number of independent survey programmes including *GALEX* MIS, *VST* KiDS, *VISTA* VIKING, *WISE*, *Herschel-ATLAS*, *GMRT*, and *ASKAP* providing UV to radio coverage. GAMA was funded by the Science and Technology Facilities Council (STFC) (UK), the Australian Research Council (ARC) (Australia), the Australian Astronomical Observatory (AAO), and the participating institutions. The GAMA website is <http://www.gama-survey.org/>. This paper has made extensive use of the TOPCAT software package (Taylor 2005).

DATA AVAILABILITY

The data underlying this paper are available at: <http://www.gama-survey.org/dr4/>.

REFERENCES

- Abramson L. E., Kelson D. D., Dressler A., Poggianti B., Gladders M. D., Oemler A., Jr, Vulcani B., 2014, *ApJ*, 785, 36
- Aihara H. et al., 2011, *ApJS*, 193, 29
- Baldry I. K. et al., 2018, *MNRAS*, 474, 3875
- Barrera-Ballesteros J. K. et al., 2021, *ApJ*, 909, 131
- Beeston R. A. et al., 2018, *MNRAS*, 479, 1077
- Bell E. F., de Jong R. S., 2000, *MNRAS*, 312, 497
- Bell E. F., Barnaby D., Bower R. G., de Jong R. S., Harper D. A., Hereld M., Loewenstein R. F., Rauscher B. J., 2000, *MNRAS*, 312, 470
- Bell E. F., Baugh C. M., Cole S., Frenk C. S., Lacey C. G., 2003, *MNRAS*, 343, 367
- Bell E. F. et al., 2012, *ApJ*, 753, 167
- Bellstedt S. et al., 2020a, *MNRAS*, 496, 3235
- Bellstedt S. et al., 2020b, *MNRAS*, 498, 5581
- Bellstedt S. et al., 2021, *MNRAS*, 503, 3309
- Bigieli F., Leroy A., Walter F., Brinks E., de Blok W. J. G., Madore B., Thornley M. D., 2008, *AJ*, 136, 2846
- Boissier S. et al., 2008, *ApJ*, 681, 244
- Bremer M. et al., 2018, *MNRAS*, 476, 12
- Casura S. et al., 2022, *MNRAS*, submitted
- Curti M., Mannucci F., Cresci G., Maiolino R., 2020, *MNRAS*, 491, 944
- Da Cunha E., Charlot S., Elbaz D., 2008, *MNRAS*, 388, 1595
- Da Cunha E., Eminian C., Charlot S., Blaizot J., 2010, *MNRAS*, 403, 1894
- Dalcanton J., Yoachim P., Bernstein R. A., 2004, *ApJ*, 608, 189
- Davies L. J. M. et al., 2016, *MNRAS*, 461, 458
- Davies L. J. M. et al., 2019, *MNRAS*, 483, 1881
- de Jong J. T. A., Verdoes Kleijn G. A., Kuijken K. H., Valentijn E. A., 2013, *Exp. Astron.*, 35, 25
- de Jong J. T. A. et al., 2017, *A&A*, 604, A134
- De Vis P. et al., 2017, *MNRAS*, 464, 4680
- De Vis P. et al., 2017, *MNRAS*, 471, 1743
- Dopita M. A., 1985, *ApJ*, 295, L5
- Driver S. P. et al., 2011, *MNRAS*, 413, 971
- Driver S. P. et al., 2016, *MNRAS*, 455, 3911
- Driver S. P. et al., 2022, *MNRAS*, 513, 419
- Eales S. et al., 2012, *ApJ*, 761, 168
- Eales S., de Vis P., Smith M. W. L., Appah K., Ciesla L., Duffield C., Schofield S., 2017, *MNRAS*, 465, 3125
- Edge A., Sutherland W., Kuijken K., Driver S., McMahon R., Eales S., Emerson J. P., 2013, *The Messenger*, 154, 32
- Ellison S. L., Patton D. R., Simard L., McConnachie A. W., 2008, *ApJ*, 672, 107
- Elmegreen B. G., 1995, *MNRAS*, 275, 944
- Freeman K. C., 1970, *ApJ*, 160, 811
- Graham A. W., Driver S. P., 2005, *Publ. Astron. Soc. Aust.*, 22, 118
- Grootes M. W. et al., 2013, *ApJ*, 766, 59
- Holwerda B. W. et al., 2019, *AJ*, 158, 103
- Holwerda B. W. et al., 2022, *MNRAS*, 513, 1972
- Hunter D. A., Elmegreen B. G., 2004, *AJ*, 128, 2170
- Jog C., Solomon P. M., 1984, *ApJ*, 276, 114
- Kennicutt R. C., 1989, *ApJ*, 344, 685
- Kennicutt R. C., 1998, *ARA&A*, 36, 189
- Kennicutt R. C., Evans N. J., 2012, *ARA&A*, 50, 531
- Lara-Lopez M. A. et al., 2013, *MNRAS*, 433, L35
- Leroy A. K., Walter F., Brinks E., Bigiel F., de Blok W. J. G., Madore B., Thornley M. D., 2008, *AJ*, 136, 2782
- Li Y., Mac Low M.-M., Klessen R. S., 2006, *ApJ*, 639, 879
- Liske J. et al., 2015, *MNRAS*, 452, 2087
- MacArthur L. A., Courteau S., Bell E., Holtzman J. A., 2004, *ApJS*, 152, 175
- Mannucci F., Cresci G., Maiolino R., Marconi A., Gnerucci A., 2010, *MNRAS*, 408, 2115
- Martig M., Bournaud F., Teyssier R., Dekel A., 2009, *ApJ*, 707, 250
- Matteucci F., Franco J., Francois P., Treyer M.-A., 1989, *Rev. Mex. Astron. Astrofis.*, 18, 145
- Moffett A. J. et al., 2016, *MNRAS*, 457, 1308
- Moffett A. J. et al., 2019, *MNRAS*, 489, 2830
- Noeske K. G. et al., 2007, *ApJ*, 660, L43
- O’Neil K., Bothun G., 2000, *ApJ*, 529, 811
- O’Neil K., Oey M. S., Bothun G., 2007, *AJ*, 134, 547
- Oemler A., Abramson L. E., Gladders M. D., Dressler A., Poggianti B. M., Vulcani B., 2017, *ApJ*, 844, 45
- Peng Y., Maiolino R., Cochrane R., 2015, *Nature*, 521, 192
- Phillipps S., Disney M. J., 1985, *MNRAS*, 217, 435
- Phillipps S., Disney M. J., Kibblewhite E. J., Cawson M. G. M., 1987, *MNRAS*, 229, 505
- Planck Collaboration XIII, 2016, *A&A*, 594, A13
- Robotham A. S. G., Taranu D. S., Tobar R., Moffett A., Driver S. P., 2017, *MNRAS*, 466, 1513
- Robotham A. S. G., Bellstedt S., Lagos C. del P., Thorne J. E., Davies L. J., Driver S. P., Bravo M., 2020, *MNRAS*, 495, 905
- Robotham A. S. G., Bellstedt S., Driver S. P., 2022, *MNRAS*, 513, 2985
- Rowlands K. et al., 2014, *MNRAS*, 441, 1017
- Salim S., Lee J. C., Ly C., Brinchmann J., Davé R., Dickinson M., Salzer J. J., Charlot S., 2014, *ApJ*, 797, 126
- Sanchez S. F., Fegan S., Giebels B., 2013, *A&A*, 554, 75
- Sanders R. L. et al., 2015, *ApJ*, 799, 138
- Schmidt M., 1959, *ApJ*, 129, 243
- Speagle J. S., Steinhardt C. L., Capak P. L., Silverman J. D., 2014, *ApJS*, 214, 15
- Taylor M. B., 2005, *ASP Conf. Ser. Vol. 347, Astronomical Data Analysis Software and Systems XIV. Astron. Soc. Pac., San Francisco*, p. 29
- Telford O. G., Dalcanton J. J., Skillman E. D., Conroy C., 2016, *ApJ*, 827, 35
- Thorne J. E. et al., 2022, *MNRAS*, 517, 6035
- Wright A. H. et al., 2016, *MNRAS*, 460, 765
- Wright A. H. et al., 2019, *A&A*, 632, A34

This paper has been typeset from a \LaTeX file prepared by the author.